Assessment of gadoxetate DCE-MRI as a biomarker of hepatobiliary transporter inhibition

Citation for the original published paper (version of record):
Ulloa, J., Stahl, S., Yates, J. et al (2013). Assessment of gadoxetate DCE-MRI as a biomarker of hepatobiliary transporter inhibition. NMR in Biomedicine, 26(10): 1258-1270.
http://dx.doi.org/10.1002/nbm.2946

(article starts on next page)

Research article

NMR IN BIOMEDICINE

Received: 15 March 2012, Revised: 14 February 2013, Accepted: 18 February 2013, Published online in Wiley Online Library: 7 April 2013

(wileyonlinelibrary.com) DOI: 10.1002/nbm.2946

Assessment of gadoxetate DCE-MRI as a biomarker of hepatobiliary transporter inhibition

Jose L. Ulloa[a], Simone Stahl[b], James Yates[c], Neil Woodhouse[a], J. Gerry Kenna[b], Huw B. Jones[d], John C. Waterton[a] and Paul D. Hockings[e,f]*

Drug-induced liver injury (DILI) is a clinically important adverse drug reaction, which prevents the development of many otherwise safe and effective new drugs. Currently, there is a lack of sensitive and specific biomarkers that can be used to predict, assess and manage this toxicity. The aim of this work was to evaluate gadoxetate-enhanced MRI as a potential novel biomarker of hepatobiliary transporter inhibition in the rat. Initially, the volume fraction of extracellular space in the liver was determined using gadopentetate to enable an estimation of the gadoxetate concentration in hepatocytes. Using this information, a compartmental model was developed to characterise the pharmacokinetics of hepatic uptake and biliary excretion of gadoxetate. Subsequently, we explored the impact of an investigational hepatobiliary transporter inhibitor on the parameters of the model *in vivo* in rats. The investigational hepatobiliary transporter inhibitor reduced both the rate of uptake of gadoxetate into the hepatocyte, k_1, and the Michaelis–Menten constant, V_{max}, characterising its excretion into bile, whereas K_M values for biliary efflux were increased. These effects were dose dependent and correlated with effects on plasma chemistry markers of liver dysfunction, in particular bilirubin and bile acids. These results indicate that gadoxetate-enhanced MRI provides a novel functional biomarker of inhibition of transporter-mediated hepatic uptake and clearance in the rat. Since gadoxetate is used clinically, the technology has the potential to provide a translatable biomarker of drug-induced perturbation of hepatic transporters that may also be useful in humans to explore deleterious functional alterations caused by transporter inhibition.

Keywords: drug-induced liver injury; DILI; DCE-MRI; liver; imaging biomarker; safety biomarker; hepatobiliary transporters; pharmacokinetic model

INTRODUCTION

Drug-induced liver injury (DILI) is responsible for up to 15% of cases of acute liver failure in Europe and the USA and is one of the leading causes of drug attrition and/or delayed progression of new drug candidates (1,2). Underlying mechanisms are still poorly understood and are difficult to identify (2,3). For many drugs that cause DILI in man, liver injury is not evident in preclinical safety studies undertaken in animals, or in early clinical trials, but is first detected only during large and expensive Phase III trials or after the drug has reached the market and a very large number of patients has been exposed (4). Typically, the first indications of liver dysfunction are asymptomatic raised plasma levels of hepatic enzymes such as aspartate aminotransferase (AST) and alanine aminotransferase (ALT) (5). Although these signals are considered useful for identification of drugs that have the potential to cause DILI in the human population, it is important to recognise that they provide no information on the mechanisms that underlie DILI. In addition, for the majority of patients who exhibit hepatic enzyme elevations the liver dysfunction is transient and is not followed by symptomatic DILI, even if drug treatment is continued (4,5). However, a small proportion of patients who exhibit hepatic enzyme elevations may subsequently develop DILI, which in some instances can result in life threatening liver failure (3). Currently, there remains an unmet need for novel biomarker approaches that can provide useful mechanistic insights and, for patients who exhibit hepatic enzyme elevations, can distinguish between individuals who are at risk of DILI and those for whom the liver dysfunction is transient or compensatory.

* *Correspondence to: Paul D. Hockings, Science and Validation, Personalised Healthcare and Biomarkers, AstraZeneca, Mölndal, Sweden. E-mail: paul.hockings@astrazeneca.com*

a *J. L. Ulloa, N. Woodhouse, J. C. Waterton*
Science and Validation, Personalised Healthcare and Biomarkers, AstraZeneca, Macclesfield, UK

b *S. Stahl, J. G. Kenna*
Molecular Toxicology, Safety Assessment UK, AstraZeneca, Macclesfield, UK

c *J. Yates*
DMPK, Oncology iMed, AstraZeneca, Macclesfield, UK

d *H. B. Jones*
Pathology, Safety Assessment UK, AstraZeneca, Macclesfield, UK

e *P. D. Hockings*
Science and Validation, Personalised Healthcare and Biomarkers, AstraZeneca, Mölndal, Sweden

f *P. D. Hockings*
MedTech West, Chalmers University of Technology, Gothenburg, Sweden

Abbreviations used: *ALT, alanine aminotransferase; AST, aspartate aminotransferase; Bsep, bile salt export pump; CKA, chemokine receptor antagonist; DCE-MRI, dynamic contrast-enhanced MRI; DILI, drug-induced liver injury; DMSO, dimethyl sulfoxide; EES, extravascular extracellular space; ES, extracellular space; Mrp2, multidrug resistance-associated protein 2; OATP, organic anion transporting polypeptide; SEM, standard error of the mean.*

In man, the most frequent observed patterns of DILI are hepatocellular (i.e. affecting hepatocytes), cholestatic (affecting bile flow and the biliary system) and mixed hepatocellular/cholestatic (where features of both hepatocellular and cholestatic injury are evident) (4,5). Hepatocellular DILI poses particular clinical concern, since for some drugs this may result in substantial loss of hepatocyte mass and development of liver failure. In contrast, the major clinical consequences of cholestatic DILI are chronic liver dysfunction arising from sustained impairment of bile flow, which may result in hepatic or biliary fibrosis, cirrhosis or vanishing bile duct syndrome (6,7).

In recent years, an emerging body of evidence has highlighted the critical role played by hepatic transporters in uptake and biliary clearance of drugs and endogenous molecules (Fig. 1). Uptake of many drugs from blood plasma through the basolateral membrane into the hepatocyte is mediated by a family of multispecific organic anion transporting polypeptides (OATPs), which also mediate uptake of some bile salts and various metabolites (8,9). Many drugs have been found to inhibit the activities of hepatic OATP uptake transporters, and this process has the potential to cause drug–drug interactions that result in altered drug pharmacokinetics (10,11). In addition, drugs, their metabolites and numerous endogenous metabolites are secreted from hepatocytes into bile via specific ATP-dependent active transport processes such as the multidrug resistance-associated protein 2 (MRP2) (12,13). Genetically determined defects in MRP2 activity have been shown to result in elevated levels of conjugated bilirubin in plasma but not overt liver injury in humans (Dubin–Johnson syndrome) (14,15), and in some strains of rats (16,17). Bile salts are excreted into bile primarily by the bile salt export pump (BSEP), and genetically inherited defects in BSEP expression and BSEP activity result in cholestatic liver injury in humans (14,15). It has been observed that many drugs that cause cholestatic or mixed hepatocellular/cholestatic DILI inhibit BSEP activity (18–20). In view of this, it has been proposed that, in patients who develop liver injury caused by such drugs, inhibition of BSEP activity results in accumulation of bile salts within hepatocytes to cytotoxic levels, thereby leading to cholestatic liver injury (21).

In view of the observed association between hepatic biliary transport inhibition by drugs and increased risk of both drug–drug interactions and DILI, approaches that can be used to quantify transporter inhibition *in vitro* have been developed and are now starting to be utilised by drug developers. However, it is important to note that, at present, the effectiveness of this approach is limited by an incomplete scientific understanding of the relationship between biliary transporter inhibition *in vitro*, the functional consequences *in vivo* and the risk of developing DILI (19). This is due in large part to the restricted range of tools that are currently available to quantify hepatic transporter interactions *in vivo*, both in preclinical species and in man. The approaches used currently require highly invasive procedures (e.g. bile duct cannulation) or provide only indirect and mechanistically non-specific evidence of liver dysfunction (e.g. evaluation of plasma levels of bile salts, conjugated bilirubin, AST, ALT etc.). There is therefore an urgent need for improved *in vivo* approaches that can be used to study hepatobiliary transporter function. Non-invasive imaging techniques, such as MRI, are well placed to fill this gap.

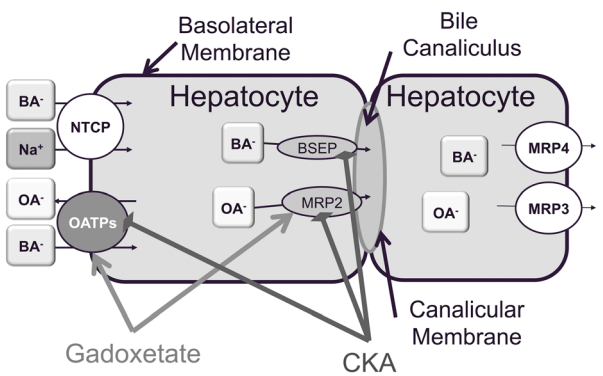

Figure 1. Overview of some of the uptake and efflux transporters expressed at the basolateral and canalicular membrane of hepatocytes. CKA, chemokine receptor antagonist compound; see text for details. OATP, organic anion transporting polypeptide; BA, bile acids; OA, organic anions; BSEP, bile salt export pump; MRP, multidrug resistance-associated protein; NTCP, Na^+ taurocholate co-transporting polypeptide.

Dynamic contrast-enhanced MRI (DCE-MRI) allows characterisation of functional aspects of physiology by adding a temporal dimension to the spatial information provided by MRI. DCE-MRI studies are normally performed using gadolinium-based contrast agents, which can be classified as extracellular (e.g. gadopentetate) or intracellular (e.g. gadoxetate), depending on their biodistribution in the body (22). Gadopentetate is a clinically approved ionic gadolinium chelate that after injection quickly distributes into the extracellular space and is completely cleared through the kidney (23,24). Gadoxetate is a clinically approved (25–27) hepatobiliary-specific MRI contrast agent (28–30). It is a lipophilic gadolinium chelate, which is excreted by both liver and kidney, in proportions that are species dependent (30). In rats, gadoxetate clearance is 70% biliary and 30% renal (28), while in humans 50% is excreted via each route (25). Gadoxetate utilises organic anion transport systems *in vivo*, since hepatic uptake is inhibited by bromosulfophthalein, bilirubin and rifampicin (29–32). *In vitro* experiments have shown that gadoxetate uptake is mediated by the liver-specific cell transporters human OATP1B1, OATP1B3 and Na^+ taurocholate co-transporting polypeptide (NTCP) (20), and rat Oatp1a1 (previously called Oatp1) (33). *In vivo* experiments in TR^- rats have shown that biliary efflux of gadoxetate is mediated by Mrp2 (31,34).

Gadoxetate has been used to measure liver function in rodent experimental models of liver fibrosis (35,36), fatty liver and bile duct obstruction (37,38). In rats, we have recently demonstrated that administration of estradiol 17-β-D-glucuronide, which is a well characterised cholestatic agent that impairs OATP, Mrp2 and Bsep function (9,20,39,40), transiently prolonged gadoxetate-induced MRI liver enhancement (39). In man, gadoxetate has been used successfully to detect and characterise liver lesions (41–46) because it is specifically taken up by hepatocytes but not tumour cells.

In the present study we have developed a novel model that describes the uptake of gadoxetate from the extracellular space into the hepatocyte and excretion into bile. We first used gadopentetate DCE-MRI to calculate the volume fraction of extracellular space in rat liver and spleen. This information was required by the model to enable estimation of the intracellular concentration of gadoxetate in the liver. We then used the model to quantify the hepatic uptake and excretion of gadoxetate in the rat, in the presence and absence of an investigational chemokine receptor antagonist (CKA) compound that we have found to inhibit biliary transporter activity *in vitro*. Our results indicate that this technique provides a novel approach for investigation of drug-induced perturbation of hepatic transporters *in vivo*.

MATERIALS AND METHODS

Animal preparation and imaging procedure

All experiments were conducted in compliance with licences issued under the UK Animals (Scientific Procedures) Act 1986 after review by the local ethics committee.

Male Han Wistar rats (232–340 g, Harlan, Bicester, UK) were fasted overnight and anaesthetised using 3% isoflurane in air. Anaesthesia was maintained at 1.5–2.0% throughout the imaging procedure. The tail vein was cannulated with a 26G catheter and flushed with heparin solution to prevent clotting (100 IU/ml in saline). Throughout the imaging procedure, rectal temperature and respiration rate were monitored (SA Instruments, New York, USA) and maintained at 37 °C and 50-60 breaths/min, respectively.

MRI was performed at 4.7 T (Oxford Instrument, Oxford, UK) incorporating a high power gradient set (200 mT/m, 121 mm inner diameter); Avance III, Bruker Biospin, Ettlingen, Germany, a 72 mm quadrature birdcage volume transceiver and Paravision 5.1 (Bruker Biospin). The imaging protocol included IntraGate FLASH (47) coronal images for anatomical reference of the abdominal cavity, an inversion recovery FISP (48,49) sequence for R1 mapping of the abdomen and IntraGate FLASH for DCE-MRI (see Table 1). Five minutes after the DCE-MRI acquisition commenced, the contrast agent (see following paragraphs) was administered intravenously (i.v.) via the tail vein with an automatic pump (5 ml/min, 305 piston pump, Gilson, Luton, UK).

We first estimated the volume fraction of extracellular space in the liver. Five healthy rats (282 ± 9 g) were imaged following the protocol described in the previous paragraph and dosed i.v. with 100 μmol/kg of gadopentetate (Magnevist, Bayer Schering Pharma, Berlin, Germany). DCE-MRI data were continuously acquired for 45 min. After the imaging session, animals were euthanised with an overdose of isoflurane.

Second, we characterised the hepatic clearance of gadoxetate when co-administered with an inhibitor of biliary transporter activity (50). Thirty rats (body weight 298 ± 26 g), with six rats per group, were dosed orally with either the chemokine antagonist (CKA) 1-(4-chloro-3-trifluoromethyl-benzyl)-5-hydroxy-1-H-indole-2-carboxylic acid (51) or vehicle. The CKA was synthesised by AstraZeneca and had a purity of more than 99%. The CKA was formulated as suspensions in the vehicle (water containing 0.5% (w/v) hydroxypropyl-methylcellulose/0.1% (w/v) polysorbate 80) and was dosed by oral gavage at 20, 200, 500 or 2000 mg/kg.

Thirty minutes after administration of CKA or vehicle, animals were anaesthetised and imaged following the protocol described in Table 1. After a further 30 min (i.e. 60 min after the CKA or vehicle dose) DCE-MRI data acquisition commenced, and 5 min later 25 μmol/kg of gadoxetate (Primovist, Bayer Schering Pharma) was administered i.v. DCE-MRI data were acquired continuously for a total of 60 min. The start of DCE-MRI acquisition was defined as $t = 0$ min, injection of gadoxetate was $t = 5$ min and the end of DCE-MRI acquisition was $t = 60$ min. At the end of the imaging session, animals were euthanised with an overdose of isoflurane and blood and liver tissue samples were taken for analysis.

Plasma chemistry analysis

Blood samples were taken from the *vena cava* into lithium-heparin tubes and the plasma fraction was separated by centrifugation at 1200 *g* and 4 °C for 10 min. Plasma samples were analysed on a Roche P Modular analyser (Roche Diagnostics, Burgess Hill, West Surrey, UK) using a total bilirubin assay, an alanine aminotransferase (ALAT/GPT) assay (both from Roche Diagnostics) and a total bile acid assay (Alere, Stockport, UK) according to the manufacturers' instructions.

Pathology analysis

At necropsy, 3–4 mm thick slices of the left lateral, right medial and caudate lobes of the liver were taken, immersed in 10% neutral buffered formalin and fixed for 48 h prior to standard tissue processing into paraffin wax. Sections (4–5 μm thick) were stained with haematoxylin and eosin (H&E) and examined by light microscopy.

In vitro transporter analysis

Determination of inhibition of human OATP1B1 (hOATP1B1) activity

Recombinant cells expressing human OATP1B1 (HEK293-hOATP1B1) (52), prepared at the Department of Molecular Biology, AstraZeneca R&D (Charnwood, UK), were cultured in standard tissue culture plasticware in Dulbecco's modified Eagle medium (DMEM), containing 4.5 mg/ml glucose and GlutaMAX™ (Invitrogen, Paisley, UK) supplemented with 10% (v/v) heat-inactivated foetal calf serum (PAA Laboratories, Yeovil, UK) and 1 mg/ml geneticin (Invitrogen). To determine inhibition of hOATP1B1-mediated uptake of [^{3}H]-estradiol 17β-glucuronide ([^{3}H]-EG; specific activity = 50 Ci/mmol; PerkinElmer Life and Analytical Sciences, Amersham, UK), 150 000 cells/well were plated into BD Biocoat™ poly-D-lysine 24-well plates (BD Biosciences, Oxford, UK) and cultured for 2–3 days until 90% confluent. Prior to the

Table 1. Details of the experiment design (MRI protocols)

	Localiser	R1 map	DCE-MRI
Sequence	IntraGate FLASH	IR-True FISP	IntraGate FLASH
Slices	10 × 2 mm	10 × 2 mm	10 × 2 mm
TR (ms)	60.3	3.4	60.3
TE (ms)	1.4	1.5	1.4
Flip angle (°)	30	4	30
FOV (mm^2)	60 × 60	60 × 60	60 × 60
Matrix size (pixels)	256 × 256	128 × 128	256 × 256
TI (ms)	–	241 + 430*n* (*n* = 0, . . ., 14)	–
Time resolution (min/vol)	–	–	1

assay, cells were washed three times with warm (37 °C) transport buffer (Hank's Balanced Salt Solution, 10 mM HEPES, pH 7.4) and pre-incubated for 15–30 min at 37 °C with transport buffer containing 3 or 30 μM CKA or dimethyl sulfoxide (DMSO) vehicle. The pre-incubation solution was replaced with transport buffer containing 20 nM [^{3}H]-EG and 3 or 30 μM CKA or DMSO vehicle. In control reactions, CKA was replaced with 30 μM cyclosporine A to determine a value for 0% activity of hOATP1B1-mediated [^{3}H]-EG uptake. The final concentration of DMSO was 0.5% (v/v) in all incubations. Each test condition was assessed in triplicate determinations. After 2 min, uptake was terminated by washing cells three times with ice-cold transport buffer and then adding 0.1% (v/v) Triton-X in water for at least 30 min to lyse the cells. The amount of [^{3}H]-EG taken up by the cells was determined via liquid scintillation counting using a TRI-CARB 3170 (PerkinElmer Life and Analytical Sciences, Waltham, MA, USA). Effects on hOATP1B1-mediated [^{3}H]-EG uptake were expressed as percentages relative to DMSO vehicle control (100%) after subtraction of background uptake in the presence of 30 μM cyclosporine A (0%). If the uptake activity in presence of test compound was below the cyclosporine A control, the activity was set to 0%.

Determination of inhibition of rat Bsep (rBsep) and rat Mrp2 (rMrp2) activity

rBsep (Abcb11) or rMrp2 (Abcc2) was expressed in *Spodoptera frugiperda Sf*21 insect cells from which membrane vesicles were prepared as described previously (19), with the modification that at the end of the preparation vesicles were re-suspended in 50 mM sucrose/10 mM HEPES/Tris pH 7.4. Abcc2 cDNA was obtained from Sprague Dawley rat liver and inserted into the pFastBac1 vector, and recombinant baculoviruses were generated with the Bac-to-Bac baculovirus expression system (Invitrogen). 100 μg vesicles were incubated with CKA or DMSO and the relevant substrate in transport buffer for 5 min at 37 °C. For rBsep 100 μg vesicles were incubated with 0.5 μM [^{3}H]-taurocholate (PerkinElmer Life and Analytical Sciences, Waltham, MA, USA) and 5 mM ATP, 20 mM $MgCl_2$, 7.7 mM HEPES/Tris pH 7.4, 141 mM KNO_3, 157 mM sucrose, 12.5 mM $Mg(NO_3)_2$. For rMrp2, 100 μg vesicles were incubated with 10 μM 5(6) carboxy 2′,7′-dichlorofluorescein (CDF; Sigma-Aldrich, Poole, UK) and 5 mM ATP, 20 mM $MgCl_2$, 7.5 mM HEPES/Tris pH 7.4, 141 mM KNO_3, 157 mM sucrose, 5 mM magnesium D-gluconate hydrate, and 0.5 mM calcium gluconate. The rMrp2 stop buffer contained 50 mM sucrose, 100 mM KCl, 5 mM HEPES/Tris pH 7.4 and 5 mM EDTA. CDF uptake into vesicles was measured by determining the relative fluorescence units (RFU) using an EnVision™ multilabel reader (PerkinElmer Life and Analytical Sciences, Waltham, MA, USA) with $\lambda_{ex/em} = 485/535$ nm. IC_{50} values were calculated from normalised data (i.e. DMSO control set to 100% transport activity and maximum inhibition observed set to 0% transport activity) with non-linear regression for a sigmoidal dose–response using the four-parameter logistic equation in GraphPad Prism version 5.00 (GraphPad Software, San Diego, CA, USA).

Calculation of gadoxetate concentration

In all the experiments, regions of interest (ROIs) covering the liver and spleen were manually selected using ImageJ (53), from both IR-FISP and DCE-MRI acquisitions, to calculate the mean longitudinal relaxation rate before contrast injection, $R_1(0)$, and to extract the time course, respectively. It was assumed that the R_1 of each organ of interest was homogeneous within the whole organ, so $R_1(0)$ represents the mean pre-contrast longitudinal relaxation over the ROI. The mean post-contrast longitudinal relaxation over the ROI, $R_1(t)$, was calculated from the IntraGate FLASH images using the signal equation of a saturation recovery spoiled gradient echo (54):

$$R_1(t) = -\frac{1}{T_R}\ln\left(\frac{1-a(t)}{1-a(t)\cos\theta}\right) \quad [1]$$

with T_R and θ the repetition time and flip angle of the IntraGate FLASH acquisition, respectively, and $a(t)$ defined by (54)

$$a(t) = \frac{S_{post}(t)(1-\exp(-T_R R_1(0)))}{S_{pre}(1-\cos\theta\exp(-T_R R_1(0)))} \quad [2]$$

with S_{pre} and $S_{post}(t)$ the average signal intensity over the ROI of the baseline (i.e. pre-injection) and post-injection at a given dynamic time point, t, respectively.

It has been shown that in tumours (55,56) and organs such as skeletal muscle (57) and brain (58), the intercompartmental water exchange is not negligible, and the system departs from the fast exchange limit regime (FXL), in which case the relationship between $R_1(t)$ and the concentration of the contrast agent becomes non-linear (59–62). However, in the hepatocyte, the mean intracellular lifetime of a water molecule ($\tau_i = 40$–50 ms (63,64)) and the water permeability coefficient ($P = 66.4 \times 10^{-4}$ cm/s (63)) are comparable to the corresponding values in an erythrocyte ($\tau_i = \sim 10$ ms, $P = 50 \times 10^{-4}$ cm/s), which is indeed in the FXL regime (57). Therefore the signal intensity can be converted to the concentration of extracellular contrast agent using the linear relationship (65)

$$C_{ES}(t) = \frac{R_1(t) - R_1(0)}{r_1 v_e} \quad [3]$$

where $C_{ES}(t)$ represents the mean extracellular concentration of contrast agent across the ROI, v_e the volume fraction of extracellular space (ES) accessible by the contrast agent and r_1 the relaxivity of the contrast agent. The relaxivities of gadoxetate and gadopentetate in liver and spleen at 4.7 T were assumed to be the same as in plasma and equal to 5.9 and 3.8 /s / mM, respectively (66).

Multicompartmental models have been used to describe the kinetics of extracellular Gd-based MRI contrast agents (55,59–62,67–69). Standard kinetic models usually consider three main compartments (69): plasma, extravascular extracellular space (EES) and intracellular compartments. However, in the case of a highly vascularised and perfused organ such as liver or spleen, where capillaries are highly permeable, the transfer exchange of contrast agent between plasma and EES occurs very fast (i.e. $K^{trans} \rightarrow \infty$ (68)), reducing it to two compartments: the extracellular space, comprising plasma and interstitial space (70,71), and the intracellular compartment, comprising hepatocytes and other liver cells, although we assume most of the intracellular space is occupied by hepatocytes (72). Following the reference region model approach (65), the extracellular concentration in the liver can be calculated by using another highly vascularised tissue, such as spleen, as the reference tissue.

For extracellular contrast agents the calculation of C_{ES} from the MRI signal in the organ of interest is straightforward using Equation [3] if v_e is known. v_e can be estimated as the area under the curve (AUC) ratio between plasma and tissue concentrations:

$$v_{e,\text{tissue}} = \frac{\int_0^t C_{\text{tissue}}(t')dt'}{\int_0^t C_{\text{plasma}}(t')dt'} \quad [4]$$

with $C_{\text{plasma}}(t)$ derived from the concentration of contrast agent in the whole blood, $C_{\text{blood}}(t)$, corrected for the haematocrit, Hct: $C_{\text{plasma}}(t) = C_{\text{blood}}(t)/(1 - \text{Hct})$. We have used this to measure the volume of extracellular space in liver and spleen with gadopentetate, which remains extracellular in these two tissues (71).

In later experiments examining gadoxetate uptake into hepatocytes we use the signal in the spleen to estimate C_{ES}. Compared with measuring C_{ES} from the blood signal in a major artery or vessel, the spleen offers the advantage of higher signal to noise ratio, larger region of interest and reduced need to include saturation bands in the MRI acquisition. Therefore we use

$$C_{\text{liver}}(t) = \frac{v_{e,\text{liver}}}{v_{e,\text{spleen}}} C_{\text{spleen}}(t) \quad [5]$$

with $C_{\text{liver}}(t)$ and $C_{\text{spleen}}(t)$ the extracellular concentrations in liver and spleen, as derived from the MRI acquisition (i.e. $C_{\text{tissue}}(t) = v_e C_{\text{ES}}(t)$, where $C_{\text{ES}}(t)$ is the 'true' extracellular concentration in the tissue).

In the case of an intracellular tracer, the total concentration in the liver, $C_t(t)$, is the combination of the concentration in both the ES and intracellular (i.e. hepatocyte) compartments:

$$C_t(t) = v_{e,\text{liver}} C_{\text{ES}}(t) + (1 - v_{e,\text{liver}}) C_{\text{hep}}(t) \quad [6]$$

If the system is in the FXL regime, the total concentration is determined directly from the signal intensity by using Equation [3], and the intracellular component is determined from Equation [6]. However, in this work we propose a more general approach and calculate the intracellular concentration from the equivalent signal intensity as follows.

The total MRI signal (normalised to baseline) in a voxel, $S(t)$, is made up of the contributions from each compartment (55):

$$S(t) = v_e S_e(t) + v_i S_i(t) \quad [7]$$

with $S_{e,i}(t)$ and $v_{e,i}$ the signal intensity and measures of the water spaces in the extracellular (e) and intracellular (i) compartments, respectively (note that outside the FXL regime Equation [7] acquires a more complex form, with v_e and v_i ($=1 - v_e$) replaced by a_S and a_L defined in (60)).

The equivalent concentration in the hepatocyte, $C_{\text{hep}}(t)$, is obtained by solving Equations [1]–[3] for the intracellular component in Equation [7]. Given that the equivalent extracellular concentration in the liver, $C_{\text{es}}(t)$, is known (Equation [5]), the extracellular signal intensity in the liver is determined by solving backwards Equations [1]–[3]. The fraction of the signal intensity in the intracellular compartment can easily be determined if we know the total signal intensity in the liver, its fraction in the extracellular space and the fractional water spaces on each compartment.

Non-linear compartmental model

Gadoxetate undergoes both renal (i.e. linear) and biliary (i.e. non-linear, Michaelis–Menten) elimination (28,73). In rats, the pharmacokinetics of gadoxetate plasma concentration can be well described by a model with central and peripheral compartments (28–30,32,74). This model assumes that elimination from a central plasma compartment follows first order kinetics in the kidney and Michaelis–Menten kinetics in the hepatobiliary system (28,29,74). In humans, a two compartment model was proposed with first order kinetics to describe gadoxetate uptake from the liver ES compartment into a hepatobiliary compartment consisting of hepatocytes and biliary ductules (75) with no efflux.

Here, we propose a two compartment model that follows the Tofts and Kermode formulation (67) to characterise the kinetics of gadoxetate clearance in the liver in terms of the rate of unidirectional uptake from the liver ES compartment into hepatocytes and the Michaelis–Menten constants of its efflux into bile.

We can therefore isolate the intracellular compartment and characterise gadoxetate kinetics in the hepatocyte (Fig. 2) using the concentrations in each compartment derived in the previous section. The model defined in Figure 2 is expressed mathematically by a non-linear differential equation (73,74):

$$\frac{dC_{\text{hep}}(t)}{dt} = k_1 C_{\text{ES}}(t) - \frac{V_{\max} C_{\text{hep}}(t)}{K_M + C_{\text{hep}}(t)} \quad [8]$$

with $C_{\text{hep}}(0) = 0$, k_1 the uptake rate of gadoxetate from the extracellular space into the hepatocyte (i.e. Oatp1a1), and the Michaelis–Menten constants of biliary efflux $V_{\max}$ (the maximum rate of efflux into bile) and K_M (the concentration of gadoxetate when the rate of efflux is half the maximum rate, i.e. $V_{\max}/2$). These three parameters reflect the effect of the CKA on the kinetics of gadoxetate transport (76), and they are estimated for each dose group by solving the following minimisation problem:

$$\min_{(k_1, V_{\max}, K_M) > 0} \left\| C_{\text{hep}}(t) - \widehat{C_{\text{hep}}}(t) \right\| \quad [9]$$

$C_{hep}(t)$ is determined by solving Equation [8] with the initial condition $C_{\text{hep}}(0) = 0$, $\widehat{C_{\text{hep}}}(t)$ represents the actual measurement from the MRI data and $\|\cdot\|$ the second norm operator. Note the non-negativity constraint in all three parameters.

Parameter estimation was performed in MATLAB (R2011a, MathWorks, Natick, MA, USA) using the optimization and differential equation toolboxes.

Statistical analysis

The significance of the effect of the CKA on the kinetics of gadoxetate uptake (k_1) and clearance ($V_{\max}$ and K_M) was investigated via ANOVA analysis (77) of the logarithm of each parameter, where variability was expressed in 95% confidence limits (CLs). Normality and homoscedasticity (i.e. variance homogeneity) of the data were confirmed via the Shapiro–Wilk normality test (78) and the Bartlett test of homogeneity of variances (79), respectively (95% CL). When comparing multiple sample groups in which marked changes were detected (95% CL), a multicomparison Tukey test (80) was performed to identify which of these differences were statistically significant. The directions of the changes were assessed with a one tailed *t*-test for the means between pairs of adjacent groups.

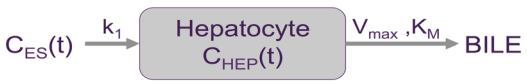

Figure 2. Two compartments that describe the kinetics of gadoxetate in the hepatocyte. k_1 characterises the uptake from the extracellular space into the hepatocyte and the Michaelis–Menten constants $V_{\max}$ and K_M characterise the gadoxetate efflux from the hepatocyte into bile.

NMR IN BIOMEDICINE

All the statistical analyses were performed in R v2.13.0 (81), using the *stats* and *agricolae* (http://tarwi.lamolina.edu.pe/~fmendiburu/) packages.

RESULTS

Estimation of the volume fraction of extracellular space in liver

Figure 3(a) shows the mean gadopentetate concentration data over time (five animals) in liver, spleen and blood following i.v. administration of the contrast agent. Using Equation [4] and a haematocrit value of 0.45, the estimated liver and spleen fractional extracellular spaces were equal to 0.23 ± 0.02 and 0.43 ± 0.02 (mean $\pm$ standard error of the mean (SEM)), respectively ($p < 0.001$ for the difference in extracellular spaces). Figure 3(b) shows that the liver gadopentetate time course can be represented by the spleen data scaled to an equivalent ES value. The blood data are included for reference.

Inhibition of transporter activity *in vitro*

Inhibition of human OATP1B1 (hOATP1B1) was determined in a stably transfected HEK293 cell line that overexpressed the transporter using the probe substrate [^{3}H]-estradiol 17β-glucuronide ([^{3}H]-EG) (52). At concentrations of 3 and 30 μM CKA, the remaining hOATP1B1-mediated [^{3}H]-EG uptake activity was 1% and 0% (mean of one experiment per test condition performed in triplicate), respectively, i.e. the activity of the transporter was completely inhibited. The effects of the CKA on ATP-dependent transporter activity of rat Bsep (rBsep) and rat Mrp2 (rMrp2) were determined using membrane vesicle assays and transporter selective probe substrates (Fig. 4). The CKA inhibited [^{3}H]-taurocholate uptake into vesicles expressing rBsep with an IC_{50} value of 129.7 μM (95% CL of geometric mean 109.8–153.2; $n = 5$) and CDF uptake into vesicles expressing Mrp2 with an IC_{50} value of 68.5 μM (95% CL of geometric mean 58.2–80.7; $n = 4$).

Evaluation of effects of CKA on hepatic clearance of gadoxetate *in vivo*

Figure 5(a) shows representative images from three rats treated by oral gavage with vehicle, CKA at 200 mg/kg or CKA at 500 mg/kg, at baseline ($t = 0$) and five time points after subsequent i.v. injection of the contrast agent gadoxetate ($t = 6$, 18, 30, 42 and 60 min). Compared with animals treated with vehicle, a marked and dose-dependent reduction in the rate of gadoxetate uptake into the liver and clearance from the liver into the GI tract was evident in animals treated with 200 and 500 mg/kg CKA. It is especially notable that enhancement of the small bowel lumen and also reflux of gadoxetate into the stomach was observed in the vehicle-treated animal. In contrast, no enhancement of the bowel was detected in the animal treated with 500 mg/kg CKA.

Figure 5(b)–(d) shows the time course of the gadoxetate concentration in the liver, spleen and hepatocytes as determined by Equation [9] (time courses are the mean over the ROI within each group and error bars represent SEM).

As can be seen in Figure 5(c), after about 30 min the amplitude of the spleen signal was comparable to the noise level in the vehicle- and lower-dose-treated animals. In order to minimise the contribution of this noise to the parameter estimation, a bi-exponential function (67) was fitted to the spleen data and used as $C_{spleen}(t)$ in Equation [5]. The concentration of gadoxetate in the hepatocyte (Figure 5(d)) was derived from its equivalent signal intensity using Equation [3]. The signal intensity in the hepatocyte was calculated from the signal intensity in liver and spleen (measured from the gadoxetate data) and the volume fraction of ES (calculated from the gadopentetate data) using Equation [7].

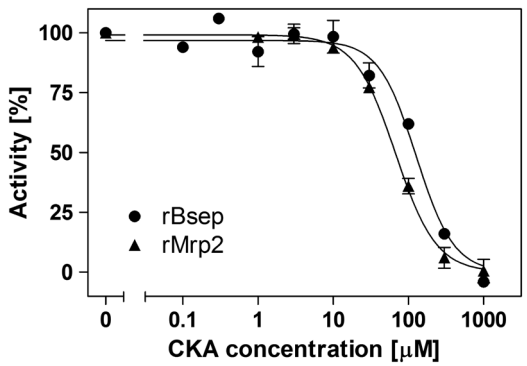

Figure 4. Inhibition of rBsep and rMrp2 transport activity by the CKA in membrane vesicles *in vitro*. Data are mean ± SEM of five (rBsep) or four (rMrp2) separate test occasions.

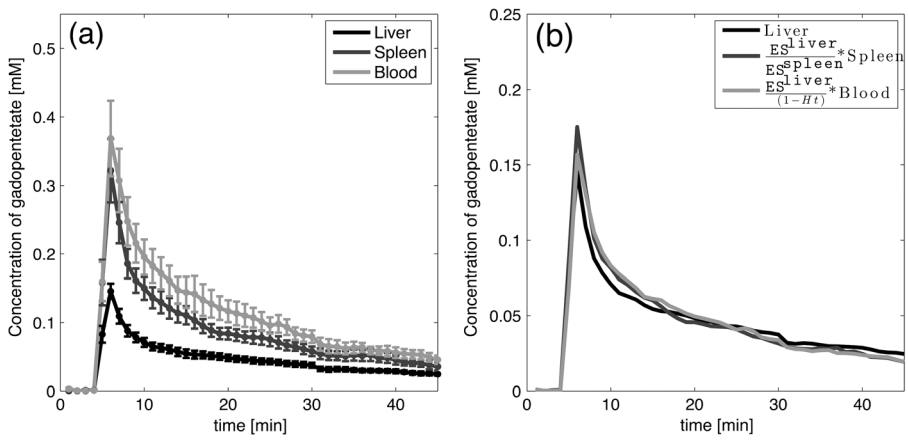

Figure 3. (a) Concentration of gadopentetate in liver, spleen and blood; solid lines represent the mean concentration and the bars the SEM over the five animals. (b) Concentration of gadopentetate in ES in liver, equivalent signal scaled from the spleen data and, for reference, the equivalent signal scaled from blood data.

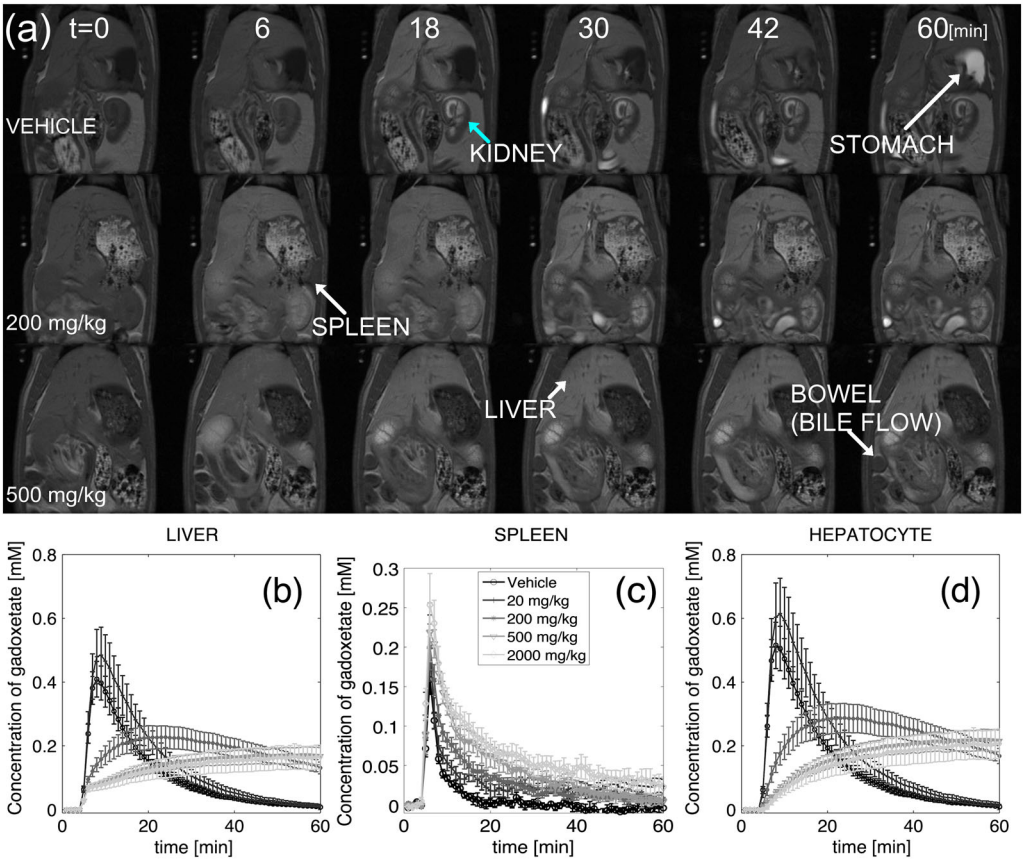

Figure 5. (a) Examples of dynamic images for animals treated with vehicle (top), 200 mg/kg (middle) or 500 mg/kg (bottom) CKA at $t = 0$, 6, 18, 30, 42 and 60 min after contrast injection. Note the enhancement of the small bowel lumen at about 30 min after contrast injection and also the reflux of gadoxetate into the stomach at the end of the acquisition in the vehicle treated animal. No enhancement was observed in the bowel of the animal treated with 500 mg/kg CKA. (b)–(d) Mean concentration of gadoxetate over ROIs covering (b) liver, (c) spleen and (d) hepatocytes. Bars represent SEM.

In Figure 6(a)–(c), representative plots of the fitting results obtained from rats treated with vehicle, or with CKA at 200 mg/kg or 500 mg/kg, are shown. The calculated rate of uptake into hepatocytes, k_1, and the Michaelis–Menten constants, V_{max} and K_M, for its biliary excretion in all dose groups are summarised in Figure 6(d)–(f) and are listed in Table 2. The data analysis showed no significant effect on the kinetic parameters caused by CKA administration at 20 mg/kg ($p = 0.23$, 0.46 and 0.44 for the differences compared with vehicle in k_1, V_{max} and K_M, respectively), whereas all three parameters were altered in rats dosed with CKA at 200 mg/kg, 500 mg/kg or 2000 mg/kg. In particular, there was a marked dose-dependent reduction in k_1 and V_{max} from 20 mg/kg to 200 mg/kg ($p = 0.002$ and 0.003 for k_1 and V_{max}, respectively) and from 200 mg/kg to 500 mg/kg ($p = 0.009$ and 0.037 for k_1 and V_{max}, respectively). No significant differences were observed between the changes in all three parameters in rats dosed with CKA at 500 mg/kg and 2000 mg/kg ($p = 0.14$, 0.56 and 0.33 for the differences in k_1, V_{max} and K_M, respectively).

In vivo clinical chemistry and pathology findings

Evaluation of H&E-stained liver sections by light microscopy (Figure 7(a)–(c)) demonstrated that only one out of six animals dosed with 2000 mg/kg CKA exhibited significant centrilobular hepatocellular degeneration and necrosis, which was accompanied by neutrophil infiltration and associated sinusoidal congestion (Figure 7(b)). This was observed in the right median lobe section only and is illustrative of acute intoxication. Other liver lobe tissue sections from this animal resembled those from all other animals in this group (e.g. Figure 7(c)) and did not show any overt changes attributable to CKA treatment. Liver sections from rats given CKA at doses of 20, 200 or 500 mg/kg displayed no histological features indicative of drug-induced hepatotoxicity.

Increases in plasma markers indicative of functional hepatobiliary impairment, i.e. total bilirubin and bile acids, exhibited marked dose-dependent increases following administration of CKA (Figure 7(d),(e)). There was also a dose-related increase in plasma ALT levels in CKA-treated animals, indicating enzyme leakage from damaged liver cells, although data for individual animals were more variable than for other plasma chemistry parameters, and this was most evident in the groups treated with 500 and 2000 mg/kg CKA (Figure 7(f)).

A striking correlation was evident between CKA-induced elevations in plasma bile acids and total bilirubin and the effects of CKA administration on kinetic parameters of hepatic uptake and biliary excretion of gadoxetate (Fig. 8). In contrast, there was no correlation between the observed increases in plasma ALT levels and the hepatic uptake rate k_1 ($r^2 = 0.44$) or the biliary efflux K_M ($r^2 = 0.41$).

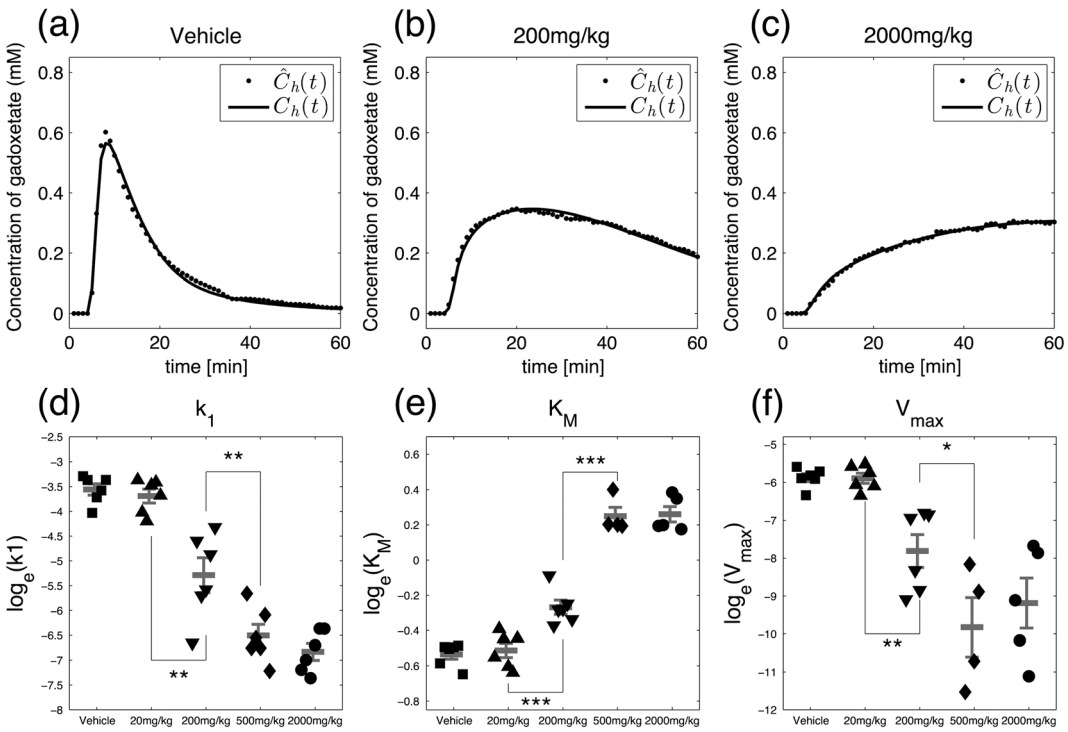

Figure 6. (a)–(c) Output of the pharmacokinetic model of hepatic clearance of gadoxetate (solid line) compared with the actual data extracted from the MR images (dotted line) for three representative animals treated with (a) vehicle, (b) 200 mg/kg CKA or (c) 500 mg/kg CKA. (d)–(f) Parameters of the model for individual animals in each group: (d) rate of uptake into the hepatocyte, k_1, (e) rate of efflux into bile, V_{max}, and (f) Michaelis–Menten constant, K_M. Each symbol represents an individual animal; mean ± SEM is also given for each group. Significance codes: *** $p < 0.001$, ** $p < 0.01$, * $p < 0.05$.

Table 2. Summary of the pharmacokinetic parameters that characterise the hepatic clearance of gadoxetate (mean ± SEM). Gadoxetate accumulates in the liver because the uptake rate, k_1, is one to two orders of magnitude larger than the efflux rate, V_{max}, producing liver enhancement in the MR images

Groups	k_1 (μmol/s)	V_{max} (μmol/s)	K_M (μM)
Vehicle	29.4 ± 3.0	2.9 ± 0.3	586.8 ± 15.4
20 mg/kg	26.1 ± 3.3	2.9 ± 0.4	601.3 ± 24.2
200 mg/kg	6.6 ± 1.9	0.6 ± 0.2	768.0 ± 32.4
500 mg/kg	1.7 ± 0.4	0.1 ± 0.1	1288.6 ± 68.1
2000 mg/kg	1.2 ± 0.2	0.1 ± 0.1	1302.8 ± 58.3

DISCUSSION

Our investigations have shown that DCE-MRI with gadoxetate provides highly robust and reproducible data to evaluate hepatic transporter function in anesthetised rats *in vivo*. We have also presented a novel non-linear two compartment model that describes the kinetics of hepatic uptake and biliary excretion of gadoxetate in the hepatocyte.

Gadoxetate is formed by including the lipophilic ethoxybenzyl moiety (EOB) to the extracellular MRI contrast agent gadopentetate, which results in hepatocyte-specific uptake of gadoxetate (28,33). When constructing the model, we therefore assume that gadoxetate does not access the intracellular space of non-hepatocytes, and that its concentration in the extracellular space of the liver is equivalent to its concentration in the extracellular space of other organs (e.g. spleen) (33,34,75). The relative volume fraction of extracellular space between liver and spleen was estimated by using gadopentetate. We then used this information to estimate the intracellular, i.e. hepatocyte, concentration of gadoxetate and to determine the parameters of the non-linear model that enabled us to characterise its hepatic uptake and excretion kinetics.

The results we have obtained indicate that this model provides a simplified but effective description of hepatic transport of gadoxetate. The parameters provided by the model were its rate of hepatocyte uptake (k_1) and the Michaelis–Menten values for biliary efflux (K_M and V_{max}). Using this approach, we have been able to explore the use of gadoxetate DCE-MRI to investigate functional effects on hepatobiliary transporter function *in vivo*. We have used a CKA test compound, which was found to inhibit the hepatobiliary transporters OATP1B1 (the human orthologue of rat Oatp1a1), Mrp2 and Bsep *in vitro*.

Although the DCE-MRI imaging data cannot in themselves provide definitive insight into the mechanism of transporter inhibition, it is clear that both a marked dose-dependent reduction of gadoxetate uptake into the liver and efflux from the hepatocyte are observed in the images in the presence of the CKA. The dose-dependent inhibition of hepatic uptake by the CKA, represented by k_1, is indicative of inhibition of organic anion uptake transporter proteins, most likely Oatp1a1, since gadoxetate was previously identified as a substrate for this transporter (21). Although it is unknown which of the rodent Oatps is the counterpart of human OATP1B1, members of the OATP/Oatp family have similar substrate and inhibitor specificities, with some exceptions (82,83). It is therefore conceivable that the inhibitory

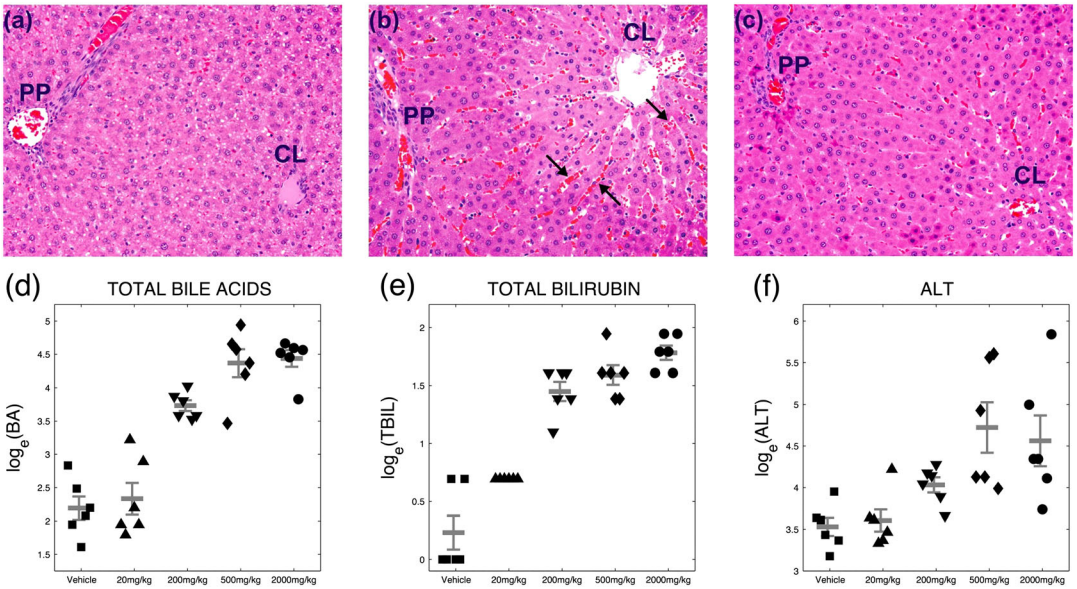

Figure 7. (a)–(c) Images of liver sections stained with haematoxylin and eosin: (a) vehicle-treated animal, (b) animal treated with 2000 mg/kg CKA showing centrilobular hepatocellular degeneration and necrosis (pale area) and sinusoidal congestion (arrows) and (c) animal treated with 2000 mg/kg CKA without drug induced findings. CL, centrilobular; PP, periportal. (d)–(f) Plasma chemistry parameters for individual animals in each group: (d) total bile acids, BA, (e) total bilirubin, TBIL, and (f) alanine aminotransferase, ALT. Mean ± SEM are also given for each group.

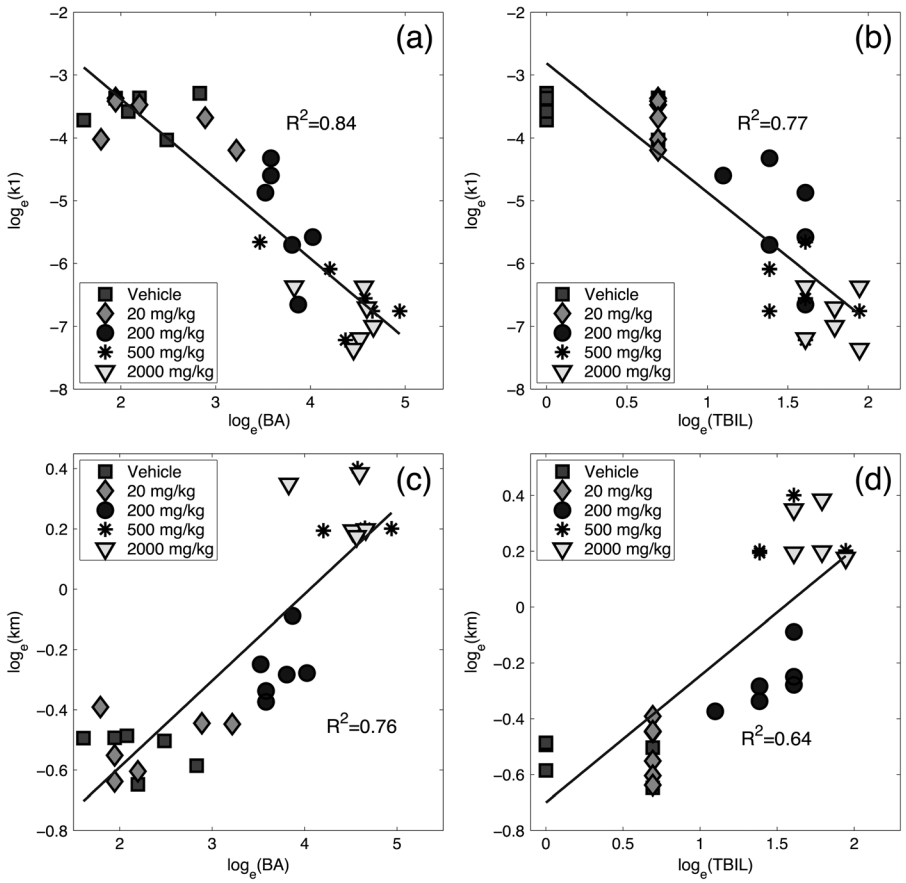

Figure 8. (a, b) Correlation of gadoxetate k_1 and plasma marker concentrations of (a) total bile acids, BA, and (b) total bilirubin, TBIL. (c, d) Correlation of gadoxetate KM and plasma marker concentrations of (c) total bile acids, BA, and (d) total bilirubin, TBIL. Each symbol represents an individual animal.

effect of the CKA on hOATP1B1, which we observed *in vitro*, also applies to the rat ortholo.gue *in vivo*. The MRI signal enhancement observed in the liver is a consequence of accumulation of gadoxetate in hepatocytes due to reduced efflux into bile caused by inhibition of Mrp2 by the CKA. These *in vivo* data are supported by the *in vitro* Bsep and Mrp2 inhibition data obtained

and by a report that gadoxetate is a substrate of Mrp2 (34). The calculated increase in the K_M of biliary efflux of gadoxetate is suggestive of competitive inhibition by the CKA (76).

The observed effects of the CKA on the kinetics of hepatic clearance of gadoxetate are consistent with previous studies in rats, where administration of OATP inhibitors such as bromosulfophthalein, rifamycin, bilirubin, prednisolone, doxorubicin hydrochloride, cisplatin, propranolol hydrochloride and rifampicin resulted in a reduction of maximum hepatic MRI signal enhancement (28,29,84–87). This highlights the potential of gadoxetate MRI to be a useful tool for evaluation of the drug–drug interaction potential of pharmaceuticals. In particular, drugs that interact with members of the OATP family have been demonstrated to have clinically relevant interactions leading to altered pharmacokinetics and potentially toxicity (11,88). Although a recent study in healthy volunteers did not show a statistically significant difference in relative liver MRI signal enhancement in subjects receiving the OATP inhibitor erythromycin compared with control subjects (89), the concept has not yet been explored with other clinically relevant drugs in man. This approach has potential benefit in the early phases of clinical trials when a liver safety signal is seen that is consistent with hepatobiliary transport inhibition and subsequent cholestasis, but it is not clear whether the signal is transient and compensation will occur or whether the patient or volunteer will progress to liver damage. In this situation an assay of *in vivo* hepatobiliary transporter function could enable more effective decision making.

Given the short duration of the study, overt cellular damage is not expected at this time point, which is reflected in a relatively poor correlation observed between the effects of CKA administration on gadoxetate hepatic transport kinetics and plasma ALT levels. Elevated serum levels of ALT reflect leakage of the enzyme from damaged cells (primarily hepatocytes) and not hepatobiliary transporter function. In fact, only a single animal in the study (dosed with CKA at 2000 mg/kg) showed necrosis and centrilobular hepatocellular degeneration (i.e. cellular damage) together with a markedly elevated plasma ALT value (344 IU/l). In contrast, we observed a close correlation between the effects of CKA compound administration on gadoxetate hepatic transport kinetics and plasma markers of hepatobiliary clearance, i.e. levels of bile acids and bilirubin. This finding provides further confirmation that administration of CKA inhibits hepatobiliary transporter function *in vivo* and is consistent with the data demonstrating inhibition of Mrp2 and Bsep by the compound *in vitro*. It also demonstrates that gadoxetate DCE-MRI is a much more sensitive technique for exploration of functional hepatobiliary transport inhibition than liver histopathology, as is evaluation of plasma levels of bile acids and bilirubin. It must be noted that, although the acquisition of DCE-MRI data was started one hour before the blood samples were taken, they strongly correlated with a decrease in the hepatic uptake rate k_1. This might suggest that gadoxetate DCE-MRI could be an earlier biomarker of impaired hepatic transporter activity than soluble plasma markers.

The plasma bile acid elevations caused by CKA administration can be attributed to the known inhibitory effect of the CKA on Bsep activity and have been observed with other drugs (90–92). These data also raise the intriguing possibility that inhibition of Bsep activity *in vivo* by the CKA administration might have contributed to the observed inhibition of biliary gadoxetate excretion, but possible transport of gadoxetate by Bsep has not been investigated. The elevated plasma bilirubin levels are likely to be a consequence of inhibition of hepatic uptake of bilirubin and its glucuronide form via OATPs (93,94) and of inhibition of biliary excretion of conjugated bilirubin by Mrp2 (95).

In recent years, evidence has been accumulated that suggests that impaired function of hepatobiliary transporters such as BSEP and MRP2, either through drug-induced inhibition or genetically determined reduction of activity, plays a role in drug-induced liver injury (19,96,97). Furthermore, inhibition of OATPs and MRP2 is associated with drug-induced hyperbilirubinaemia (98,99), and drug–drug interactions related to certain OATPs have clinical relevance (11). Consequently, candidate drugs are frequently assessed for transporter interactions during drug discovery using *in vitro* approaches. A major challenge when attempting to understand the functional significance of such *in vitro* data is that the relationship between inhibition of transporter activity by drugs *in vitro* and potential deleterious functional effects *in vivo* remains ill defined (100). This highlights the urgent need for new approaches that can be used to generate such understanding. Our results suggest that gadoxetate DCE-MRI may be a suitable technique for this purpose, especially where this is complemented by evaluation of bile acids and bilirubin as plasma biomarkers. In the future it will be important to generate data in animals treated with a broad range of different test compounds exhibiting a range of potency and selectivity of transport inhibition in order to develop a more complete understanding of the consequences that may ensue *in vivo*. In addition, gadoxetate MRI has been used extensively in the clinic (41–46), which raises the possibility that the approach might also be useful during drug development, to aid in clinical hazard identification and risk assessment of novel candidate drugs.

CONCLUSION

This study has shown that gadoxetate DCE-MRI enables quantification of drug-induced alterations in hepatobiliary transporter activity in the rat *in vivo*. Administration to rats of a test compound (CKA) that inhibited the activity of the hepatic transporters OATP, Bsep and Mrp2 *in vitro* resulted in changes in the kinetics of gadoxetate clearance that could be explained in terms of effects on three parameters: the rate of gadoxetate uptake into hepatocytes, k_1, and the Michaelis–Menten constants for efflux from hepatocytes into bile, V_{max} and K_M. These changes correlated closely with effects of CKA compound on serum biomarkers indicative of biliary transporter inhibition (total bile acids and bilirubin). We conclude that gadoxetate DCE-MRI can detect inhibition of hepatobiliary transporters and has the potential to serve as a novel biomarker of functional cholestasis. Furthermore, since gadoxetate is used in the clinic, it provides a novel approach that is potentially applicable both in laboratory animals and in patients in order to support safety evaluation of novel pharmaceuticals.

Acknowledgements

We thank Guy Healing, Matthew Smith, Charlotte Warrender and Gareth Parker for excellent technical assistance, Laura Beattie, Jacqueline Caddy and Gail Tracey for analysis of plasma samples, the Formulation and Analytical Support Group, Safety Assessment UK, for preparation of the dosing solutions of the CKA and Pradeep Sharma for his contribution supporting the hOATP1B1 assessment. We also thank Peter Webborn for critical review of the manuscript and Edvin Johansson for very useful discussions.

REFERENCES

1. Abboud G, Kaplowitz N. Drug-induced liver injury. Drug Saf. 2007; 30: 277–294.
2. Holt MP, Ju C. Mechanisms of drug-induced liver injury. AAPS J. 2006; 8: E48–54.
3. Marschall HU, Wagner M, Zollner G, Trauner M. Clinical hepatotoxicity. Regulation and treatment with inducers of transport and cofactors. Mol. Pharm. 2007; 4: 895–910.
4. Maddrey WC. Drug-induced hepatotoxicity: 2005. J. Clin. Gastroenterol. 2005; 39: S83–89.
5. Aithal GP, Watkins PB, Andrade RJ, Larrey D, Molokhia M, Takikawa H, Hunt CM, Wilke RA, Avigan M, Kaplowitz N, Bjornsson E, Daly AK. Case definition and phenotype standardization in drug-induced liver injury. Clin. Pharmacol. Ther. 2011; 89: 806–815.
6. Andrade RJ, Lucena MI, Kaplowitz N, Garcia-Munoz B, Borraz Y, Pachkoria K, Garcia-Cortes M, Fernandez MC, Pelaez G, Rodrigo L, Duran JA, Costa J, Planas R, Barriocanal A, Guarner C, Romero-Gomez M, Munoz-Yague T, Salmeron J, Hidalgo R. Outcome of acute idiosyncratic drug-induced liver injury: long-term follow-up in a hepatotoxicity registry. Hepatology 2006; 44: 1581–1588.
7. Desmet VJ. Vanishing bile duct syndrome in drug-induced liver disease. J. Hepatol. 1997; 26 (Suppl. 1): 31–35.
8. Hagenbuch B, Gui C. Xenobiotic transporters of the human organic anion transporting polypeptides (OATP) family. Xenobiotica 2008; 38: 778–801.
9. Smith NF, Figg WD, Sparreboom A. Role of the liver-specific transporters OATP1B1 and OATP1B3 in governing drug elimination. Expert Opin. Drug Metab. Toxicol. 2005; 1: 429–445.
10. Fahrmayr C, Fromm MF, Konig J. Hepatic OATP and OCT uptake transporters: their role for drug–drug interactions and pharmacogenetic aspects. Drug Metab. Rev. 2010; 42: 380–401.
11. International Transporter Consortium, Giacomini KM, Huang SM, Tweedie DJ, Benet LZ, Brouwer KL, Chu X, Dahlin A, Evers R, Fischer V, Hillgren KM, Hoffmaster KA, Ishikawa T, Keppler D, Kim RB, Lee CA, Niemi M, Polli JW, Sugiyama Y, Swaan PW, Ware JA, Wright SH, Yee SW, Zamek-Gliszczynski MJ, Zhang L. Membrane transporters in drug development. Nat. Rev. Drug Discov. 2010; 9: 215–236.
12. Jemnitz K, Heredi-Szabo K, Janossy J, Ioja E, Vereczkey L, Krajcsi P. ABCC2/Abcc2: a multispecific transporter with dominant excretory functions. Drug Metab. Rev. 2010; 42: 402–436.
13. Nies AT, Schwab M, Keppler D. Interplay of conjugating enzymes with OATP uptake transporters and ABCC/MRP efflux pumps in the elimination of drugs. Expert Opin. Drug Metab. Toxicol. 2008; 4: 545–568.
14. Elferink RO, Groen AK. Genetic defects in hepatobiliary transport. Biochim. Biophys. Acta 2002; 1586: 129–145.
15. Pauli-Magnus C, Stieger B, Meier Y, Kullak-Ublick GA, Meier PJ. Enterohepatic transport of bile salts and genetics of cholestasis. J. Hepatol. 2005; 43: 342–357.
16. Buchler M, Konig J, Brom M, Kartenbeck J, Spring H, Horie T, Keppler D. cDNA cloning of the hepatocyte canalicular isoform of the multidrug resistance protein, cMrp, reveals a novel conjugate export pump deficient in hyperbilirubinemic mutant rats. J. Biol. Chem. 1996; 271: 15 091–15 098.
17. Paulusma CC, Bosma PJ, Zaman GJ, Bakker CT, Otter M, Scheffer GL, Scheper RJ, Borst P, Oude Elferink RP. Congenital jaundice in rats with a mutation in a multidrug resistance-associated protein gene. Science 1996; 271: 1126–1128.
18. Horikawa M, Kato Y, Tyson CA, Sugiyama Y. Potential cholestatic activity of various therapeutic agents assessed by bile canalicular membrane vesicles isolated from rats and humans. Drug Metab. Pharmacokinet. 2003; 18: 16–22.
19. Dawson S, Stahl S, Paul N, Barber J, Kenna JG. In vitro inhibition of the bile salt export pump correlates with risk of cholestatic drug-induced liver injury in humans. Drug Metab. Dispos. 2012; 40: 130–138.
20. Stieger B, Fattinger K, Madon J, Kullak-Ublick GA, Meier PJ. Drug- and estrogen-induced cholestasis through inhibition of the hepatocellular bile salt export pump (Bsep) of rat liver. Gastroenterology 2000; 118: 422–430.
21. Perez MJ, Briz O. Bile-acid-induced cell injury and protection. World J. Gastroenterol. 2009; 15: 1677–1689.
22. Geraldes CF, Laurent S. Classification and basic properties of contrast agents for magnetic resonance imaging. Contrast Media Mol. Imaging 2009; 4: 1–23.
23. Goldstein HA, Kashanian FK, Blumetti RF, Holyoak WL, Hugo FP, Blumenfield DM. Safety assessment of gadopentetate dimeglumine in U.S. clinical trials. Radiology 1990; 174: 17–23.
24. Kieffer SA. Gadopentetate dimeglumine: observations on the clinical research process. Radiology 1990; 174: 7–8.
25. Hamm B, Staks T, Muhler A, Bollow M, Taupitz M, Frenzel T, Wolf KJ, Weinmann HJ, Lange L. Phase I clinical evaluation of Gd-EOB-DTPA as a hepatobiliary MR contrast agent: safety, pharmacokinetics, and MR imaging. Radiology 1995; 195: 785–792.
26. Reimer P, Rummeny EJ, Shamsi K, Balzer T, Daldrup HE, Tombach B, Hesse T, Berns T, Peters PE. Phase II clinical evaluation of Gd-EOB-DTPA: dose, safety aspects, and pulse sequence. Radiology 1996; 199: 177–183.
27. Bluemke DA, Sahani D, Amendola M, Balzer T, Breuer J, Brown JJ, Casalino DD, Davis PL, Francis IR, Krinsky G, Lee FT, Jr, Lu D, Paulson EK, Schwartz LH, Siegelman ES, Small WC, Weber TM, Welber A, Shamsi K. Efficacy and safety of MR imaging with liver-specific contrast agent: U.S. multicenter phase III study. Radiology 2005; 237: 89–98.
28. Weinmann HJ, Schuhmann-Giampieri G, Schmitt-Willich H, Vogler H, Frenzel T, Gries H. A new lipophilic gadolinium chelate as a tissue-specific contrast medium for MRI. Magn. Reson. Med. 1991; 22: 233–237; discussion 242.
29. Clement O, Muhler A, Vexler V, Berthezene Y, Brasch RC. Gadolinium-ethoxybenzyl-DTPA, a new liver-specific magnetic resonance contrast agent. Kinetic and enhancement patterns in normal and cholestatic rats. Invest. Radiol. 1992; 27: 612–619.
30. Schuhmann-Giampieri G, Schmitt-Willich H, Press WR, Negishi C, Weinmann HJ, Speck U. Preclinical evaluation of Gd-EOB-DTPA as a contrast agent in MR imaging of the hepatobiliary system. Radiology 1992; 183: 59–64.
31. Weinmann HJ, Bauer H, Frenzel T, Muhler A, Ebert W. Mechanism of hepatic uptake of gadoxetate disodium. Acad. Radiol. 1996; 3 (Suppl. 2): S232–234.
32. Schuhmann-Giampieri G, Schmitt-Willich H, Frenzel T, Schitt-Willich H [corrected to Schmitt-Willich H]. Biliary excretion and pharmacokinetics of a gadolinium chelate used as a liver-specific contrast agent for magnetic resonance imaging in the rat. J. Pharm. Sci. 1993; 82: 799–803.
33. van Montfoort JE, Stieger B, Meijer DK, Weinmann HJ, Meier PJ, Fattinger KE. Hepatic uptake of the magnetic resonance imaging contrast agent gadoxetate by the organic anion transporting polypeptide Oatp1. J. Pharmacol. Exp. Ther. 1999; 290: 153–157.
34. Muhler A, Oude Elferink RPJ, Weinmann HJ. Complete elimination of the hepatobiliary MR contrast agent Gd-EOB-DTPA in hepatic dysfunction: An experimental study using transport-deficient, mutant rats. MAGMA 1993; 1: 134–139.
35. Tsuda N, Matsui O. Paradoxical correlation between Mrp2 expression and fibrosis. In *Proceedings 19th Scientific Meeting*. International Society for Magnetic Resonance in Medicine: Montreal, 2011; 391.
36. Ryeom HK, Kim SH, Kim JY, Kim HJ, Lee JM, Chang YM, Kim YS, Kang DS. Quantitative evaluation of liver function with MRI using Gd-EOB-DTPA. Korean J. Radiol. 2004; 5: 231–239.
37. Schmitz SA, Muhler A, Wagner S, Wolf KJ. Functional hepatobiliary imaging with gadolinium-EOB-DTPA. A comparison of magnetic resonance imaging and ^{153}gadolinium-EOB-DTPA scintigraphy in rats. Invest. Radiol. 1996; 31: 154–160.
38. Ni Y, Marchal G, Lukito G, Yu J, Muhler A, Baert AL. MR imaging evaluation of liver enhancement by Gd-EOB-DTPA in selective and total bile duct obstruction in rats: correlation with serologic, microcholangiographic, and histologic findings. Radiology 1994; 190: 753–758.
39. Ulloa J, Stahl S, Liess C, Bright J, McDermott A, Woodhouse N, Halliday J, Parmar A, Healing G, Kenna G, Holmes A, Barjat H, Waterton JC, Hockings PD. Effects of a single intravenous dose of estradiol-17β D-glucuronide on biliary excretion: assessment with gadoxetate DCE-MRI. In *Proceedings 18th Scientific Meeting*. International Society for Magnetic Resonance in Medicine: Stockholm, 2010; 2593.
40. Kanai N, Lu R, Bao Y, Wolkoff AW, Vore M, Schuster VL. Estradiol 17 beta-D-glucuronide is a high-affinity substrate for oatp organic anion transporter. Am. J. Physiol. 1996; 270: F326–331.
41. Fukukura Y, Kamiyama T, Takumi K, Shindo T, Kumagai Y, Nakajo M. Contrast-enhanced MR cholangiography with Gd-EOB-DTPA: visualization of the biliary ducts in comparison with HASTE MR cholangiography. In *Proceedings 17th Scientific Meeting*. International Society for Magnetic Resonance in Medicine: Honolulu, 2009; 4076.

42. Carlos RC, Hussain HK, Song JH, Francis IR. Gadolinium-ethoxybenzyl-diethylenetriamine pentaacetic acid as an intrabiliary contrast agent: preliminary assessment. AJR Am. J. Roentgenol. 2002; 179: 87–92.
43. Huppertz A, Haraida S, Kraus A, Zech CJ, Scheidler J, Breuer J, Helmberger TK, Reiser MF. Enhancement of focal liver lesions at gadoxetic acid-enhanced MR imaging: correlation with histopathologic findings and spiral CT – initial observations. Radiology 2005; 234: 468–478.
44. Filippone A, Blakeborough A, Breuer J, Grazioli L, Gschwend S, Hammerstingl R, Heinz-Peer G, Kittner T, Laghi A, Leen E, Lencioni R, Lucidarme O, Remplik P, Robinson PJ, Ruehm SG, Schaefer F, Stoupis C, Tombach B, Valette PJ, Zech CJ, Huppertz A. Enhancement of liver parenchyma after injection of hepatocyte-specific MRI contrast media: a comparison of gadoxetic acid and gadobenate dimeglumine. J. Magn. Reson. Imaging 2010; 31: 356–364.
45. Chung SH, Kim MJ, Choi JY, Hong HS. Comparison of two different injection rates of gadoxetic acid for arterial phase MRI of the liver. J. Magn. Reson. Imaging 2010; 31: 365–372.
46. Choi JY, Choi JS, Kim MJ, Lim JS, Park MS, Kim JH, Chung YE. Detection of hepatic hypovascular metastases: 3D gradient echo MRI using a hepatobiliary contrast agent. J. Magn. Reson. Imaging 2010; 31: 571–578.
47. Bishop J, Feintuch A, Bock NA, Nieman B, Dazai J, Davidson L, Henkelman RM. Retrospective gating for mouse cardiac MRI. Magn. Reson. Med. 2006; 55: 472–477.
48. Scheffler K, Hennig J. T(1) quantification with inversion recovery TrueFISP. Magn. Reson. Med. 2001; 45: 720–723.
49. Schmitt P, Griswold MA, Jakob PM, Kotas M, Gulani V, Flentje M, Haase A. Inversion recovery TrueFISP: quantification of T(1), T(2), and spin density. Magn. Reson. Med. 2004; 51: 661–667.
50. Ulloa J, Stahl S, Woodhouse N, Healing G, Kenna G, Waterton JC, Hockings P. Assessment of DCE-MRI with gadoxetate as a biomarker of drug induced cholestasis. In *Proceedings 19th Scientific Meeting*. International Society for Magnetic Resonance in Medicine: Montreal, 2011; 1534.
51. Faull AW, Kettle JG. Indole derivatives as MCP-1 receptor antagonists. WIPO Patent Application WO/2001/051466. 19 July 2001.
52. Sharma P, Holmes VE, Elsby R, Lambert C, Surry D. Validation of cell-based OATP1B1 assays to assess drug transport and the potential for drug–drug interaction to support regulatory submissions. Xenobiotica 2010; 40: 24–37.
53. Abramoff MD, Magelhaes PJ, Ram SJ. Image processing with ImageJ. Biophotonics International 2004; 11: 36–42.
54. Haacke EM, Filleti CL, Gattu R, Ciulla C, Al-Bashir A, Suryanarayanan K, Li M, Latif Z, DelProposto Z, Sehgal V, Li T, Torquato V, Kanaparti R, Jiang J, Neelavalli J. New algorithm for quantifying vascular changes in dynamic contrast-enhanced MRI independent of absolute T1 values. Magn. Reson. Med. 2007; 58: 463–472.
55. Li X, Huang W, Morris EA, Tudorica LA, Seshan VE, Rooney WD, Tagge I, Wang Y, Xu J, Springer CS Jr. Dynamic NMR effects in breast cancer dynamic-contrast-enhanced MRI. Proc. Natl. Acad. Sci. USA 2008; 105: 17 937–17 942.
56. Huang W, Tudorica LA, Li X, Thakur SB, Chen Y, Morris EA, Tagge IJ, Korenblit ME, Rooney WD, Koutcher JA, Springer CS Jr. Discrimination of benign and malignant breast lesions by using shutter-speed dynamic contrast-enhanced MR imaging. Radiology 2011; 261: 394–403.
57. Landis CS, Li X, Telang FW, Molina PE, Palyka I, Vetek G, Springer CS Jr. Equilibrium transcytolemmal water-exchange kinetics in skeletal muscle in vivo. Magn. Reson. Med. 1999; 42: 467–478.
58. Quirk JD, Bretthorst GL, Duong TQ, Snyder AZ, Springer CS Jr, Ackerman JJ, Neil JJ. Equilibrium water exchange between the intra- and extracellular spaces of mammalian brain. Magn. Reson. Med. 2003; 50: 493–499.
59. Landis CS, Li X, Telang FW, Coderre JA, Micca PL, Rooney WD, Latour LL, Vetek G, Palyka I, Springer CS Jr. Determination of the MRI contrast agent concentration time course in vivo following bolus injection: effect of equilibrium transcytolemmal water exchange. Magn. Reson. Med. 2000; 44: 563–574.
60. Yankeelov TE, Rooney WD, Li X, Springer CS Jr. Variation of the relaxographic 'shutter-speed' for transcytolemmal water exchange affects the CR bolus-tracking curve shape. Magn. Reson. Med. 2003; 50: 1151–1169.
61. Li X, Rooney WD, Springer CS Jr. A unified magnetic resonance imaging pharmacokinetic theory: intravascular and extracellular contrast reagents. Magn. Reson. Med. 2005; 54: 1351–1359.
62. Yankeelov TE, Luci JJ, DeBusk LM, Lin PC, Gore JC. Incorporating the effects of transcytolemmal water exchange in a reference region model for DCE-MRI analysis: theory, simulations, and experimental results. Magn. Reson. Med. 2008; 59: 326–335.
63. Yano M, Marinelli RA, Roberts SK, Balan V, Pham L, Tarara JE, de Groen PC, LaRusso NF. Rat hepatocytes transport water mainly via a non-channel-mediated pathway. J. Biol. Chem. 1996; 271: 6702–6707.
64. Bacic G, Alameda JC Jr, Iannone A, Magin RL, Swartz HM. NMR study of water exchange across the hepatocyte membrane. Magn. Reson. Imaging 1989; 7: 411–416.
65. Yankeelov TE, Luci JJ, Lepage M, Li R, Debusk L, Lin PC, Price RR, Gore JC. Quantitative pharmacokinetic analysis of DCE-MRI data without an arterial input function: a reference region model. Magn. Reson. Imaging 2005; 23: 519–529.
66. Rohrer M, Bauer H, Mintorovitch J, Requardt M, Weinmann HJ. Comparison of magnetic properties of MRI contrast media solutions at different magnetic field strengths. Invest. Radiol. 2005; 40: 715–724.
67. Tofts PS, Kermode AG. Measurement of the blood–brain barrier permeability and leakage space using dynamic MR imaging. 1. Fundamental concepts. Magn. Reson. Med. 1991; 17: 357–367.
68. Tofts PS, Brix G, Buckley DL, Evelhoch JL, Henderson E, Knopp MV, Larsson HB, Lee TY, Mayr NA, Parker GJ, Port RE, Taylor J, Weisskoff RM. Estimating kinetic parameters from dynamic contrast-enhanced T(1)-weighted MRI of a diffusable tracer: standardized quantities and symbols. J. Magn. Reson. Imaging 1999; 10: 223–232.
69. Jackson A, Buckley DL, Parker GJM (eds). *Dynamic Contrast-Enhanced Magnetic Resonance Imaging in Oncology*. Springer: Berlin, 2005.
70. Materne R, Smith AM, Peeters F, Dehoux JP, Keyeux A, Horsmans Y, Van Beers BE. Assessment of hepatic perfusion parameters with dynamic MRI. Magn. Reson. Med. 2002; 47: 135–142.
71. Sommer W, Sourbron S, Huppertz A, Ingrisch M, Reiser M, Zech C. Contrast agents as a biological marker in magnetic resonance imaging of the liver: conventional and new approaches. Abdom. Imaging 2012; 37: 164–179.
72. Blouin A, Bolender RP, Weibel ER. Distribution of organelles and membranes between hepatocytes and nonhepatocytes in the rat liver parenchyma. A stereological study. J. Cell Biol. 1977; 72: 441–455.
73. Schuhmann-Giampieri G, Frenzel T, Schmitt-Willich H. Pharmacokinetics in rats, dogs and monkeys of a gadolinium chelate used as a liver-specific contrast agent for magnetic resonance imaging. Arzneimittelforschung 1993; 43: 927–931.
74. Schuhmann-Giampieri G. Nonlinear pharmacokinetic modeling of a gadolinium chelate used as a liver-specific contrast agent for magnetic resonance imaging. Arzneimittelforschung 1993; 43: 1020–1024.
75. Dahlqvist Leinhard O, Dahlstrom N, Kihlberg J, Sandstrom P, Brismar TB, Smedby O, Lundberg P. Quantifying differences in hepatic uptake of the liver specific contrast agents Gd-EOB-DTPA and Gd-BOPTA: a pilot study. Eur. Radiol. 2012; 22(3): 642–653.
76. Stryer L. *Biochemistry*. Freeman: San Francisco, CA, 1975.
77. Chambers JM, Hastie TJ. *Statistical Models in S*. Chapman and Hall: Pacific Grove, California, USA, 1991.
78. Royston P. Remark AS. R94: a remark on algorithm AS 181: the *W*-test for normality. J. R. Stat. Soc. C (Appl. Stat.) 1995; 44: 547.
79. Bartlett MS. Properties of sufficiency and statistical tests. Proc. R. Soc. London A, Math. Phys. Sci. 1937; 160: 268.
80. Steel R, Torrie J, Dickey D. *Principles and Procedures of Statistics: a Biometrical Approach*. McGraw-Hill: New York, USA, 1996.
81. R Development Core Team. R: a Language and Environment for Statistical Computing, Vienna, Austria, 2011.
82. Meier PJ, Eckhardt U, Schroeder A, Hagenbuch B, Stieger B. Substrate specificity of sinusoidal bile acid and organic anion uptake systems in rat and human liver. Hepatology 1997; 26: 1667–1677.
83. Hagenbuch B, Meier PJ. The superfamily of organic anion transporting polypeptides. Biochim. Biophys. Acta 2003; 1609: 1–18.
84. Kato N, Yokawa T, Tamura A, Heshiki A, Ebert W, Weinmann HJ. Gadolinium-ethoxybenzyl-diethylenetriamine-pentaacetic acid interaction with clinical drugs in rats. Invest. Radiol. 2002; 37: 680–684.
85. Shitara Y, Itoh T, Sato H, Li AP, Sugiyama Y. Inhibition of transporter-mediated hepatic uptake as a mechanism for drug–drug interaction between cerivastatin and cyclosporin A. J. Pharmacol. Exp. Ther. 2003; 304: 610–616.

86. Shitara Y, Sato H, Sugiyama Y. Evaluation of drug–drug interaction in the hepatobiliary and renal transport of drugs. Annu. Rev. Pharmacol. Toxicol. 2005; 45: 689–723.
87. Vavricka SR, Van Montfoort J, Ha HR, Meier PJ, Fattinger K. Interactions of rifamycin SV and rifampicin with organic anion uptake systems of human liver. Hepatology 2002; 36: 164–172.
88. Link E, Parish S, Armitage J, Bowman L, Heath S, Matsuda F, Gut I, Lathrop M, Collins R. SLCO1B1 variants and statin-induced myopathy – a genomewide study. N. Engl. J. Med. 2008; 359: 789–799.
89. Huppertz A, Breuer J, Fels LM, Schultze-Mosgau M, Sutter G, Klein S, Frericks B, Hamm B, Wagner M. Evaluation of possible drug–drug interaction between gadoxetic acid and erythromycin as an inhibitor of organic anion transporting peptides (OATP). J. Magn. Reson. Imaging 2011; 33: 409–416.
90. Bohme M, Muller M, Leier I, Jedlitschky G, Keppler D. Cholestasis caused by inhibition of the adenosine triphosphate-dependent bile salt transport in rat liver. Gastroenterology 1994; 107: 255–265.
91. Fattinger K, Funk C, Pantze M, Weber C, Reichen J, Stieger B, Meier PJ. The endothelin antagonist bosentan inhibits the canalicular bile salt export pump: a potential mechanism for hepatic adverse reactions. Clin. Pharmacol. Ther. 2001; 69: 223–231.
92. Funk C, Pantze M, Jehle L, Ponelle C, Scheuermann G, Lazendic M, Gasser R. Troglitazone-induced intrahepatic cholestasis by an interference with the hepatobiliary export of bile acids in male and female rats. Correlation with the gender difference in troglitazone sulfate formation and the inhibition of the canalicular bile salt export pump (Bsep) by troglitazone and troglitazone sulfate. Toxicology 2001; 167: 83–98.
93. Cui Y, Konig J, Leier I, Buchholz U, Keppler D. Hepatic uptake of bilirubin and its conjugates by the human organic anion transporter SLC21A6. J. Biol. Chem. 2001; 276: 9626–9630.
94. Briz O, Serrano MA, Maclas RI, Gonzalez-Gallego J, Marin JJ. Role of organic anion-transporting polypeptides, OATP-A, OATP-C and OATP-8, in the human placenta–maternal liver tandem excretory pathway for foetal bilirubin. Biochem. J. 2003; 371: 897–905.
95. Kamisako T, Leier I, Cui Y, Konig J, Buchholz U, Hummel-Eisenbeiss J, Keppler D. Transport of monoglucuronosyl and bisglucuronosyl bilirubin by recombinant human and rat multidrug resistance protein 2. Hepatology 1999; 30: 485–490.
96. Choi JH, Ahn BM, Yi J, Lee JH, Lee JH, Nam SW, Chon CY, Han KH, Ahn SH, Jang IJ, Cho JY, Suh Y, Cho MO, Lee JE, Kim KH, Lee MG. MRP2 haplotypes confer differential susceptibility to toxic liver injury. Pharmacogenet. Genomics 2007; 17: 403–415.
97. Daly AK, Aithal GP, Leathart JB, Swainsbury RA, Dang TS, Day CP. Genetic susceptibility to diclofenac-induced hepatotoxicity: contribution of UGT2B7, CYP2C8, and ABCC2 genotypes. Gastroenterology 2007; 132: 272–281.
98. Campbell SD, de Morais SM, Xu JJ. Inhibition of human organic anion transporting polypeptide OATP 1B1 as a mechanism of drug-induced hyperbilirubinemia. Chem. Biol. Interact. 2004; 150: 179–187.
99. Ah YM, Kim YM, Kim MJ, Choi YH, Park KH, Son IJ, Kim SG. Drug-induced hyperbilirubinemia and the clinical influencing factors. Drug Metab. Rev. 2008; 40: 511–537.
100. Kusuhara H, Sugiyama Y. In vitro–in vivo extrapolation of transporter-mediated clearance in the liver and kidney. Drug Metab. Pharmacokinet. 2009; 24: 37–52.